

Electron plasma profiles from a cathode with an r^2 potential variation

J. M. Kriesel^{a)} and C. F. Driscoll

Department of Physics and Institute for Pure and Applied Physical Sciences, University of California at San Diego, La Jolla, California 92093

(Received 11 November 1997; accepted 9 January 1998)

A simple one-dimensional model of Maxwellian injection into a cylindrical Penning–Malmberg trap is presented. This model is used to predict the radial density profile of an electron column produced by a biased cathode with an r^2 potential variation. The column density $n(r)$ is assumed to depend upon the cathode potential voltage $V_k(r)$ and the self-consistent space-charge potential $\phi(r)$ as $n(r) \propto \exp\{e[\phi(r) - V_k(r)]/T\}$. A one-parameter family of theoretical solutions describes the radial density profiles. The model's predictions agree well with electron density profiles resulting from a spiral tungsten filament measured over a wide range in cathode voltages. © 1998 American Institute of Physics. [S1070-664X(98)00805-2]

I. INTRODUCTION

Pure-electron plasmas in cylindrical Penning–Malmberg traps are routinely used for experiments on plasma waves, collisional transport, and two-dimensional (2-D) fluid flows.^{1–3} For these experiments, it is often desirable to have a quiescent and predictable initial plasma, which has a characteristic Debye length that is less than the plasma dimensions. Once trapped, the plasma can be further manipulated depending upon the experiment at hand. In an attempt to minimize the energy of the injected electrons, many experiments use a cathode with a radial potential drop that varies as r^2 . The intent is for the voltage on the cathode to match the radial space-charge potential of a uniform density column of electrons. Mismatched potentials lead to a higher plasma temperature, and therefore an undesirably large Debye length. In this paper we present a simple one-dimensional (1-D) model of electron injection from a cathode with an r^2 potential variation. Radial electron density profiles predicted by the model are compared to measurements of electron columns from a spiral filament.

We consider a cylindrically symmetric trap with a moderately strong axial magnetic field. Electrons produced from a cathode outside the trap are born with a potential $V_k(r)$ and move axially along the magnetic field lines. The more slowly moving electrons can be reflected back to the cathode by the space-charge potential, $\phi(r)$, in the trap. This is similar to the reflection of electrons from a “virtual cathode” in Langmuir’s model of Child’s law for space-charge-limited emission;⁴ however, in our model the reflecting potential is determined by a radial, not an axial, solution to Poisson’s equation.

We assume the electrons from the cathode can be described by a Maxwellian distribution with energy spread T and density $n_k(r)$. In this paper we do *not* describe the alternative case, where an energetic beam is injected into the trap. For Maxwellian injection, the density of electrons in the trap, $n(r)$, can be written as $n(r) = n_k(r) \exp\{e[\phi(r)$

$-V_k(r)]/T\}$. The trapped density profile is found by solving this equation along with Poisson’s equation for $\phi(r)$.

In one previous model of Maxwellian injection into a Penning–Malmberg trap,⁵ the electron temperature was assumed to be zero, and the cathode potential was taken to have a parabolic variation in radius, written as $V_k(r) = -V_b + V_f r^2/R_k^2$, where V_b and V_f are positive constants. With $T=0$, the potentials must match, i.e. $\phi(r) = V_k(r)$. The resulting electron density profiles are “top hats,” having a constant value, $n(r) = n_o$, out to a certain radius then dropping to zero. The magnitude of the density, n_o , is proportional to the voltage drop across the filament, V_f , while the radial extent of the plasma, R_p , and thus the total number of trapped electrons, is determined by the cathode bias voltage, V_b .

A separate model⁶ considered nonzero temperatures, but only for an equipotential cathode, i.e. $V_k(r) = -V_b$. In this case, with $T \neq 0$, some mismatch between the space-charge potential and the cathode potential is allowed. An analytic solution for the density profiles show that the resulting electron columns are “hollow,” having highest density at the column edge and lowest density at $r=0$, where the space-charge potential is most negative.

In this paper, we present a model that considers both nonzero electron temperature and a parabolic r^2 potential drop across the cathode. In addition, we also allow the cathode emission, described by $n_k(r)$, to vary as a function of radius, which is an influence not previously considered. We obtain the density profiles by integrating a modified Poisson’s equation, and find that scalings reduce the problem to a single-parameter family of solutions. This approach is similar to finding the density profiles for a pure-electron plasma in global thermal equilibrium.^{7,8}

As in the zero-temperature solutions mentioned above, the trapped electron density is proportional to V_f , while the total number of electrons is determined by V_b . In this finite-temperature model, however, the radial profiles can vary in shape and are not restricted to be “top hats.” To find the theoretical profile shape appropriate to a given experimental situation, the emission profile of the cathode, $f_k(r)$

^{a)}Electronic mail: kriesel@physics.ucsd.edu

$\equiv n_k(r)/n_k(0)$, is used to determine a family of scaled density curves. The experimental values for $n_k(0)$, V_f , V_b , and T along with values for the cathode radius, R_k , and trap radius, R_w , determine the corresponding member (from the family of curves) and the numerical values of the scaling parameters. In this way the model uses information about the cathode to determine the shape and magnitude of the electron density profile it produces in a given cylindrical trap.

We have measured the density profiles that result from a spiral cathode with an approximately parabolic potential drop and an (unintentional) off-center peak in emission. The density was found to be proportional to V_f , and the total number of trapped electrons was found to be proportional to V_b , as expected. The shape of the measured profiles, however, was somewhat surprising. The electron density was relatively low at the center and higher near the radial midpoint, resulting in a profile with multiple dips and peaks for some values of the ratio V_b/V_f . When the radial nonuniformity in cathode emission is included, the model does quite well at predicting, not only the magnitude of the density, but also the radial variations in the measured profiles over a wide range of experimental parameters. Close agreement is found, despite the fact that none of the experimental z variations due to the thermionic emission, cathode shape, or accelerating grid enter the model.

We find that the experiments do deviate from the model when the injection becomes beam-like rather than Maxwellian. In addition, when the $\mathbf{E} \times \mathbf{B}$ rotation is slow, θ variations in the injected density can persist in the trapped plasma, and our 1-D radial model fails. Thus, the model presented here should have applicability to other experimental devices with nominally θ -symmetric and Maxwellian injection processes,⁹⁻¹¹ but not to those with beam-like injection conditions^{12,13} or large azimuthal density asymmetries.^{14,15}

The remainder of the paper is organized as follows: In Sec. II we present a detailed description of the model; predicted radial density profiles for a uniformly emitting cathode are shown in Fig. 2. In Sec. III we discuss the experimental setup and measurements, and attempt to justify some of the simplifying assumptions inherent to the model. Theoretical density curves computed for our specific experimental emission profile are shown along with measured density curves in Fig. 8. In the final section we further discuss some of the assumptions and applicability of the model.

II. THEORY

Consider the basic cylindrical configuration shown in Fig. 1, and assume azimuthal symmetry. A disk-like cathode of radius R_k has an applied voltage that varies with radius as $V_k(r)$. Electrons emitted from the cathode move in the z direction along magnetic field lines which are coaxial with a series of grounded conducting cylinders of radius R_w . In the experimental apparatus, a grid prevents z -dependent space-charge effects from limiting the cathode emission. However, these z variations are not part of the model, and the effect of the grid will be ignored for the remainder of this section. In addition to motion along the magnetic field, the electrons

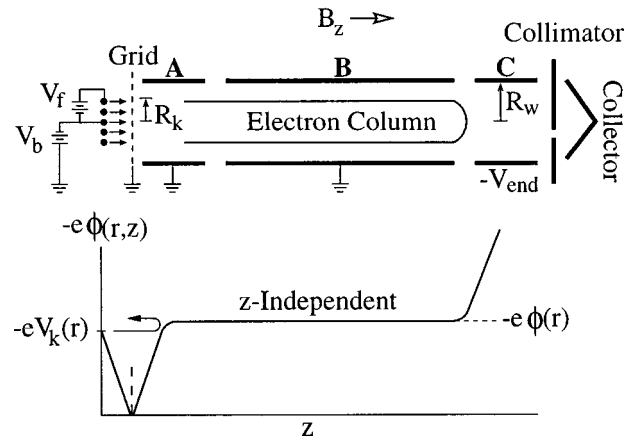


FIG. 1. Cross section of the cylindrical experimental configuration. The lower curve is a plot of the potential seen by an electron as a function of axial position, showing that some electrons are reflected back to the cathode by the z -independent space charge of the electron column. Note that $V_k(r) = \phi(r, z=0)$.

will $\mathbf{E} \times \mathbf{B}$ drift in the $\hat{\theta}$ direction due to the radial space-charge electric field; this drift is also ignored in our θ -symmetric model.

We make the essential assumption that the electrons produced by the cathode can be described by a Maxwellian distribution with thermal energy spread T and a radial density profile $n_k(r)$. We also assume that sufficient emission leads to a steady-state column of electrons in the trap. This column is long compared to its radius, allowing us to use a z -independent space-charge potential, $\phi(r)$, and a z -independent electron density, $n(r)$, to describe it. The condition of sufficient emission implies that $|\phi(r)| \geq |V_k(r)|$ for $r \leq R_k$; therefore, some electrons emitted by the cathode are reflected by the space charge of the column (as shown in Fig. 1). Those electrons that are energetic enough to enter are eventually reflected at ring C by an applied voltage, $-V_{\text{end}}$, which is substantially more negative than any interior potential.

It is the goal of the model to predict the electron column density profile from the cathode parameters. With the assumption that the distribution of electron velocities is Maxwellian and symmetric in v_z (i.e., each electron with $+v_z$ is eventually reflected to the same axial position with $-v_z$), we can use a Boltzmann relationship to relate the density and space-charge potential of electrons in the column to the density emitted by the cathode and voltage applied to the cathode. The z -independent column density is thus given by

$$n(r) = n_k(r) \exp\left(\frac{e}{T} [\phi(r) - V_k(r)]\right) \quad r \leq R_k, \\ = 0, \quad r > R_k. \quad (1)$$

The column density is also related to the space-charge potential through Poisson's equation,

$$\frac{1}{r} \frac{\partial}{\partial r} \left(r \frac{\partial \phi(r)}{\partial r} \right) = 4\pi e n(r), \quad (2)$$

where $-e$ is the electron charge. The boundary conditions are

$$\left. \frac{\partial \phi(r)}{\partial r} \right|_{r=0} = 0, \quad \phi(R_w) = 0. \tag{3}$$

Here and throughout the paper, we use cgs units, except where V and T are explicitly labelled as volts and electron-volts.

With the experimental parameters T , R_k , R_w , and $n_k(r)$ specified, Eqs. (1)–(3) can be solved numerically for $n(r)$ given any $V_k(r)$. For the specific case where $V_k(r)$ is parabolic in radius, we will demonstrate that appropriate scaling gives a one-parameter family of solutions for $n(r)$. These theoretical density profiles will be shown to provide a good match to experimental measurements.

We begin by writing the parabolic cathode potential as

$$V_k(r) = -V_b + V_f \frac{r^2}{R_k^2}, \tag{4}$$

where V_f is the voltage drop across the cathode (or filament) from center to edge, and $-V_b$ is the bias voltage at the center of the cathode, as shown in Fig. 1. We also write the density of electrons emitted by the cathode as

$$n_k(r) \equiv n_k(0) f_k(r), \tag{5}$$

where $f_k(r)$ is a function that describes possible radial variations in cathode emission. It is convenient to define a characteristic density and central Debye length as

$$n_o \equiv \frac{V_f}{e \pi R_k^2} = (2.21 \times 10^6 \text{ cm}^{-3}) \frac{V_f \text{ (Volts)}}{R_k^2}, \tag{6}$$

and

$$\lambda_{D0} \equiv \left(\frac{T}{4 \pi e^2 n(0)} \right)^{1/2} = \frac{R_k}{2} \left(\frac{T}{e V_f} \right)^{1/2} \left(\frac{n_o}{n(0)} \right)^{1/2}. \tag{7}$$

Here n_o is referred to as the ‘‘matching’’ density, because a uniform density electron column with $n(r) = n_o$ will have a radial space-charge potential variation that matches the parabolic cathode potential variation given by Eq. (4), i.e., $\phi_o(r) = \phi_o(0) + V_f r^2 / R_k^2$.

We now introduce a modified potential,

$$\psi(r) \equiv \frac{e}{T} \{ [\phi(r) - V_k(r)] - [\phi(0) - V_k(0)] \}, \tag{8}$$

so that Eqs. (1), (5), and (8) give

$$n(r) = n(0) f_k(r) e^{\psi(r)}. \tag{9}$$

Due to the finite size of the cathode, Eq. (9) is only valid for $r \leq R_k$; but here we will ignore this restriction and leave it to be reconsidered below. We next scale r to the central Debye length as $\rho \equiv r / \lambda_{D0}$, and define the parameter γ as

$$\gamma \equiv \frac{n_o}{n(0)} - 1. \tag{10}$$

Using Eqs. (2), (4), and (6)–(10) we obtain a Poisson-like equation for the modified potential ψ , as

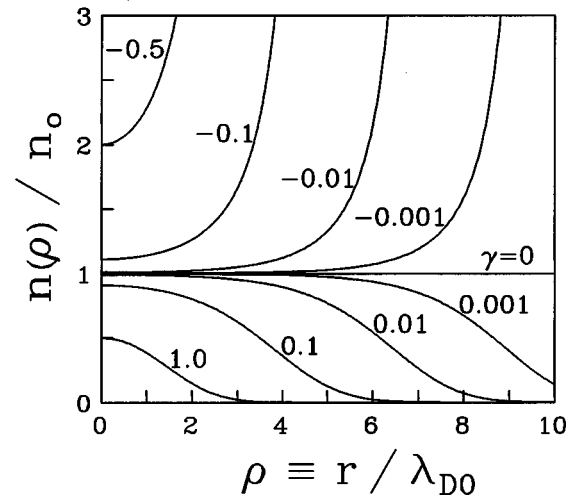


FIG. 2. Scaled theoretical density profiles from a uniformly emitting cathode of infinite radius, for various values of the parameter γ .

$$\frac{1}{\rho} \frac{\partial}{\partial \rho} \left(\rho \frac{\partial \psi(\rho)}{\partial \rho} \right) = f_k(\rho) e^{\psi(\rho)} - (1 + \gamma). \tag{11}$$

The identity $\psi(0) = 0$ and the condition for zero electric field at $r = 0$ give the boundary conditions

$$\psi(0) = 0, \quad \left. \frac{\partial \psi}{\partial \rho} \right|_{\rho=0} = 0. \tag{12}$$

Using Eqs. (11) and (12) with $f_k(\rho)$ specified, $\psi(\rho)$ can be determined numerically for different values of the single parameter γ . Using Eqs. (9) and (10) we then obtain the desired radial density profile, $n(r)$. Notice that in Eqs. (6)–(12), the explicit dependence on $n_k(0)$ has been removed and only the radial variations in emission, $f_k(\rho)$, remains.

We also note that Eqs. (9)–(11) with $f_k(\rho) = 1$ are identical to the equations used to calculate the radial density profiles of an electron plasma in thermal equilibrium.^{7,8} The similarity arises because both analyses presume that the density is proportional to a Boltzmann factor involving the difference between the plasma potential and a potential that varies as r^2 . In the thermal equilibrium equations $V_k(r)$ is replaced by an effective confining potential due to rotation in a magnetic field, and n_o is the fictitious neutralizing background ‘‘charge’’ arising from this rotation.

We now consider the general solutions to Eq. (11) with $f_k(\rho) = 1$, i.e., with a cathode that emits electrons uniformly at all radii. Using Eqs. (9) and (10), we calculate the scaled density profiles, which are shown in Fig. 2, parametrized only by the value of γ . The $\gamma = 0$ solution is the ‘‘matching’’ solution mentioned above. Here $\psi(\rho) = 0$, and the density profile is flat with $n(\rho) = n_o$ out to $\rho = \infty$. The $\gamma > 0$ solutions are bounded and go to zero as $\rho \rightarrow \infty$. However, the $\gamma < 0$ solutions become infinite at a finite radius $\rho_s(\gamma)$; this singularity point moves closer to $\rho = 0$ as γ becomes more negative.

In Fig. 2 the finite radial size of the cathode is ignored. A more realistic solution would include the restriction that $n(\rho) = 0$ for $\rho > \rho_k$, where $\rho_k \equiv R_k / \lambda_{D0}$. For the experiments discussed in the following section, $\rho_k \approx 8$. The solu-

tions in Fig. 2 with $\rho_s < \rho_k$ imply a point of infinite density within the electron column; this would violate the assumption of adequate cathode emission. However, if the singularity point falls beyond the cathode radius, i.e., $\rho_s > \rho_k$, then the singularity can be ignored.

For the thermal equilibrium solutions of Ref. 7, no unbounded $\gamma < 0$ solutions are allowed. In contrast, the electron column we are considering is “connected” to the cathode, so that the finite cathode size provides an extra boundary condition. In this case, some $\gamma < 0$ solutions are physically realizable, with the limit being the value of γ where $\rho_s = \rho_k$. Using Eqs. (7) and (10) along with the solutions to Eq. (11), we define this lower (negative) limit as γ_{\min} with

$$\rho_s(\gamma_{\min}) \equiv \rho_k(\gamma_{\min}) = 2 \left(\frac{eV_f}{T} \right)^{1/2} (1 + \gamma_{\min})^{-1/2}. \quad (13)$$

This definition in turn defines an absolute limit on the central density, which can be written as

$$n(0) < \frac{n_o}{1 + \gamma_{\min}}. \quad (14)$$

A somewhat surprising result that comes out of this definition is that for a given $f_k(r)$, the maximum scaled central density, $n(0)/n_o$, depends only on the ratio eV_f/T .

We now briefly consider the equipotential cathode for comparison. In this case $n_o = 0$, $V_f = 0$, and $\gamma = -1$. Here Eqs. (13) and (14) lose their meaning; however, an analytic solution to Eq. (11) exists,⁶ where

$$\begin{aligned} \psi(\rho) &= -2 \ln(1 - \rho^2/8), \\ n(\rho) &= n(0)(1 - \rho^2/8)^{-2}. \end{aligned} \quad (15)$$

The density profile is “hollow” and has a singularity at $\rho_s = \sqrt{8}$. The limit on the central density is found by setting $\rho_k < \rho_s$, which can be rewritten as

$$n(0) < \frac{2T}{e^2 \pi R_k^2} = (4.42 \times 10^6 \text{ cm}^{-3}) \frac{T(\text{eV})}{R_k^2}. \quad (16)$$

We return again to the parabolic potential cathode and consider the problem of determining which value of the theoretical parameter γ corresponds to a given experimental situation. To obtain this correspondence, the theoretical solutions $\psi(r)$ with boundary conditions at $r=0$ must be related to the experimental voltages V_f and V_b , which are relative to the grounded wall. We begin by calculating the space-charge potential, $\phi(\rho)$, in the zero density region beyond the cathode radius. This is done by integrating Laplace’s equation from the cathode radius to the wall, where $\phi(R_w) = 0$. By matching solutions at $\rho = \rho_k$ and using Eqs. (1), (4), and (8), the following relationship can then be written:

$$\begin{aligned} \frac{eV_b}{T} &= \ln \left(\frac{n(0)}{n_k(0)} \right) + \left(\psi(\rho_k) + \frac{eV_f}{T} \right) \\ &+ \ln \left(\frac{R_w}{R_k} \right) \left(\rho_k \frac{\partial \psi}{\partial \rho} \Big|_{\rho_k} + \frac{2eV_f}{T} \right). \end{aligned} \quad (17)$$

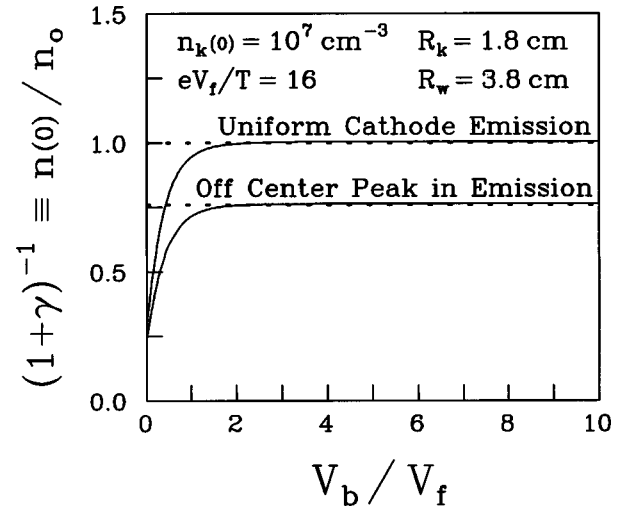


FIG. 3. Scaled central density plotted versus the ratio of bias voltage to filament voltage for a uniformly and nonuniformly emitting cathode. These curves are used to relate γ to the cathode voltages. The two dotted lines are at $\gamma = 0$ and $\gamma = 0.316$ ($\gamma^* = 0$).

The first term on the right-hand side of Eq. (17) represents the scaled potential increase on axis between the cathode and the z -independent region. This is now the only place where $n_k(0)$ enters the model, and typically this term is negligible compared to the other two. The second term represents the scaled potential increase from the center of the column to its edge, and the third term represents the scaled potential increase in the vacuum from the edge of the electron column to the grounded conducting wall.

The experimental values for R_k , R_w , and eV_f/T are typically fixed; and because of the model’s weak dependence on $n_k(0)$, this parameter can be considered fixed at some reasonable value, or even ignored altogether. We solve Eq. (11) for $\psi(r)$, given $f_k(r)$ and γ . Using Eq. (17) we can then find a one-to-one relationship between a value of γ and the ratio eV_b/T . This is more conveniently expressed as a relationship between the scaled central density, $n(0)/n_o$, and the ratio V_b/V_f (here eV_f/T is considered fixed).

The upper curve of Fig. 3 shows the dependence of the central density on the cathode bias voltage for a uniformly emitting cathode with typical experimental values for $n_k(0)$, eV_f/T , R_w , and R_k . As V_b/V_f is increased from zero, the central density increases and γ decreases. From Fig. 2, we see that this corresponds to the radial extent of the column increasing as more electrons are allowed to fill the trap. When $V_b/V_f \approx 2.5$, Fig. 3 shows that $n(0) = n_o$ and $\gamma = 0$, corresponding to the matched solution, where $\psi(\rho) = 0$ and $\partial\psi/\partial\rho = 0$ for all values of ρ . From Eq. (17) with the first term neglected, we see that, in general, this occurs at $V_b/V_f \approx 1 + 2 \ln(R_w/R_k)$. As V_b/V_f is increased past the matching point, the density profile becomes hollow and γ becomes negative. In this situation electrons preferentially fill the trap at the edge of the column where the space-charge potential is less negative. As $V_b/V_f \rightarrow \infty$, the edge density increases “without limit” corresponding to $\rho_s \rightarrow \rho_k$. However, the central density only increases to a limit slightly greater than n_o , equivalent to a γ slightly less than zero.

III. COMPARISON TO EXPERIMENTS

We have measured the trapped density profiles on an apparatus where the cathode is wound in the form of an Archimedes spiral with approximately eight turns. The radial filament potential is approximated well by Eq. (4), where V_f is the resistive voltage drop due to the heating current ($V_f \approx 10 \text{ A} \times 1.3 \Omega$), and $-V_b$ is the bias to ground provided by a separate power supply, as shown in Fig. 1. For the experiments presented here, the filament temperature was kept fixed at $T_f \approx 0.16 \text{ eV}$ (1800 K). The emission depends on the filament temperature according to the well-known Richardson–Dushman equation¹⁶ for thermionic emission. In our experiments, V_f was varied without changing the filament temperature by pulsing the heating current for the short time required to inject the electrons into the trap.

A grounded grid in front of the filament prevents the local space-charge potential from limiting the emission, but also substantially increases the energy spread of the electrons. The strong ($\approx 200 \text{ V/cm}$), spatially varying electric fields in the filament-grid region cause spatial “mixing” over distances of approximately 1 mm, which is one-half the distance between the wires of the spiral filament. Thus, the electrons are accelerated to a beam with a spread of parallel energies at the grid. When this beam is decelerated by the space-charge potential due to electrons in the trap, it slows to an approximately Maxwellian distribution with energy spread T determined largely by the turn-to-turn potential differences on the filament. We find that this energy spread is well characterized by $T \approx eV_f/16$ for $V_f > 2.6 \text{ V}$, and $T \approx 0.16 \text{ eV}$ for $V_f \leq 2.6 \text{ V}$. In essence, the spatial and trajectory averaging of the filament-grid region, together with θ averaging during the injection process, allows us to ignore the details of the spiral filament and use the continuous disk cathode model characterized by n_k and T .

The experiments are performed in an inject, dump/measure cycle. During injection, the voltages on rings A, B, and C are as shown in Fig. 1. The steady-state electron column is then “cut off” from the cathode by ramping ring A to a large negative voltage, trapping a nearly cylindrical column in ring B, which has a length $L = 36 \text{ cm}$. The ramping time ($\sim 100 \mu\text{s}$) is long compared to the $\mathbf{E} \times \mathbf{B}$ rotation time ($\sim 5 \mu\text{s}$), so the column symmetrizes in θ while still partially “connected” to the filament. Immediately after the column is trapped (within $\sim 10 \mu\text{s}$), electrode C is ramped to ground, thereby dumping the electrons to the collimator and collector along magnetic field lines. The filament and conducting cylinders are all located within a solenoid providing a uniform magnetic field of $B_z = 380 \text{ G}$.

The radial density profile of the trapped electrons is obtained by stepping the collimator hole across the column and measuring the dumped charge $Q(r)$ at each radius; the density is given by $n(r) = -Q(r)/eA_hL$, where $A_h = \pi(0.16 \text{ cm})^2$ is the collimator hole area, and L is the length of the confinement region (ring B). Since it is not known exactly where ring A “cuts” the steady-state column, our use of the confinement length to calculate the column density may produce a systematic error (most likely an underestimation of the density) by as much as 10%. The shot-

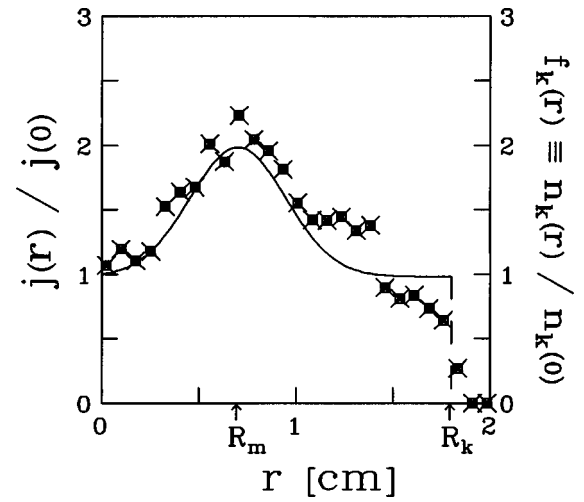


FIG. 4. Scaled cathode emission as a function of radius. The points are the scaled through-current measured with the radial collector; $j(0) \approx 3.6 \times 10^{-5} \text{ A/cm}^2$. The solid curve is the model approximation of Eq. (18).

to-shot noise, however, is typically less than 1%.

To obtain the effective emission profile $n_k(r)$ of our source, we measure the through-current $j(r)$ with ring C grounded, i.e., with no trapped electron space-charge potential. These measurements show that the emission is not uniform in r or θ . Maximum emission occurs at radius $R_m = 0.7 \text{ cm}$; this peak in emission is up to three times greater than the emission at $r=0$. The irregularity in emission is most likely due to an asymmetry in the turn-to-turn spacing, coupled with a slight peak in T_f near $r \approx R_k/2$. Since the trapping experiments are operated in such a way as to average out variations in θ , we make the approximation that the peak is symmetric in θ with a magnitude about twice that at $r=0$. We approximate the radially dependent part of the effective emission profile as

$$f_k(r) = \frac{n_k(r)}{n_k(0)} = 1 + e^{-4(r/R_m - 1)^2} - e^{-4}. \quad (18)$$

This function is plotted in Fig. 4, along with the measured $j(r)/j(0)$ at one particular value of θ . The absolute magnitude of the effective emission is determined by $j(0) = (e/2)n_k(0)(T/m_e)^{1/2}$. From the measurement $j(0) = 36 \mu\text{A/cm}^2$, we obtain $1.2 \leq n_k(0) \leq 2.7 \times 10^7 \text{ cm}^{-3}$ for $0.16 \leq T \leq 0.8 \text{ eV}$.

For any value of γ , Eqs. (10) and (7) determine λ_{D0} and allow us to scale the emission profile to $\rho = r/\lambda_{D0}$. The maximum of emission then occurs at

$$\rho_m \equiv \frac{R_m}{\lambda_{D0}} = 2 \frac{R_m}{R_k} \left(\frac{eV_f}{T} \right)^{1/2} \frac{1}{(1 + \gamma)^{1/2}}. \quad (19)$$

Since the ratios R_m/R_k and eV_f/T are fixed experimentally, the scaled radius of maximal emission depends only on γ .

Even with nonuniform emission, our model predicts the trapped electron density profiles as a family of scaled profiles parametrized solely by γ . We numerically integrate Eq. (11) with $f_k(\rho)$ given by Eq. (18) to obtain $\psi(\rho)$, and then use Eq. (9) to obtain the theoretical density profiles. Figure 5 shows the predicted density profiles for our “peaked” cathode us-

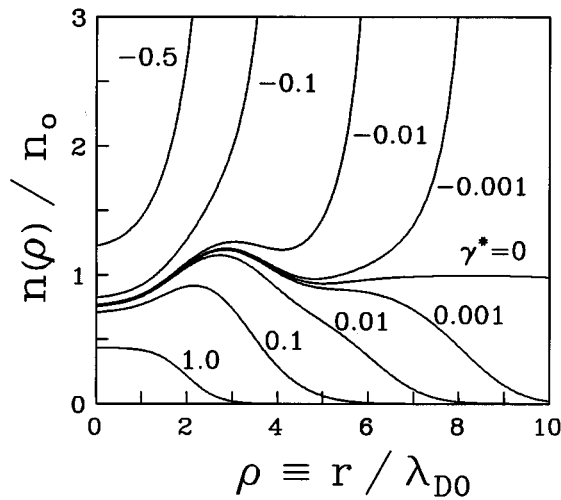


FIG. 5. Scaled theoretical density profiles for a cathode with an off-center factor-of-2 peak in emission. Curves are labeled by $\gamma^* \equiv \gamma - \gamma_0$, where $\gamma_0 \approx 0.316$ parametrizes the asymptotically flat solution analogous to the ‘‘matched solution’’ for a uniform cathode.

ing the experimental values $R_m/R_k=0.7/1.8$ and $eV_f/T=16$. The curves in Fig. 5 are labeled by γ^* , where $\gamma^* \equiv \gamma - \gamma_0$, with $\gamma_0 \approx 0.316$. The $\gamma = \gamma_0$ solution is defined to correspond to a density profile that is asymptotically flat as $\rho \rightarrow \infty$. We make the analogy between the $\gamma = 0$ ‘‘matched’’ solution for the case of uniform cathode emission, and the $\gamma^* = 0$ solution for the peaked cathode. We can carry the analogy further and say that for $\gamma^* > 0$, $n(\rho)$ is finite out to $\rho = \infty$; whereas for $\gamma^* < 0$, $n(\rho)$ has a singularity at the point $\rho = \rho_s(\gamma)$. Taking the finite cathode size into consideration, it is again possible to find limits on γ and $n(0)$ using Eqs. (13) and (14). We will return to these limits at the end of this section.

The scaled central density obtained from the nonuniform cathode is also uniquely determined by the ratio V_b/V_f , as shown by the lower curve of Fig. 3. [We took $n_k(0) = 10^7 \text{ cm}^{-3}$ for both curves of Fig. 3 as a rough estimate.] If we compare Figs. 2 and 5 to each other and the two curves of Fig. 3 to each other, we notice that an off-center peak in emission at $\rho = \rho_m$ leads to an increase in density near $\rho = \rho_m$, as one would expect. However, this increase in density near the peak in emission comes at the expense of a decrease in density near $\rho = 0$.

As a basic check to the model, we measure the line density N_L , which is the total number of electrons per unit length, as a function of the bias voltage. In Fig. 6 we scale N_L to the line density for a column of uniform density $n_0 \propto V_f$, and plot the results for two different values of V_f . The error bars are an estimate of the shot-to-shot noise. The solid theoretical curve is obtained by integrating the density profiles of Fig. 5 out to the cathode radius, i.e. $N_L = \lambda_{D0}^2 \int_0^{\rho_k} \rho d\rho n(\rho)$. The theoretical and measured values of the line density increase with bias voltage, and are in close agreement for $V_b/V_f \lesssim 4$.

The trapped line density N_L is quite insensitive to the nonuniformity in cathode emission: the curve of N_L vs V_b for a uniformly emitting cathode [i.e., integrating the $n(\rho)$ of

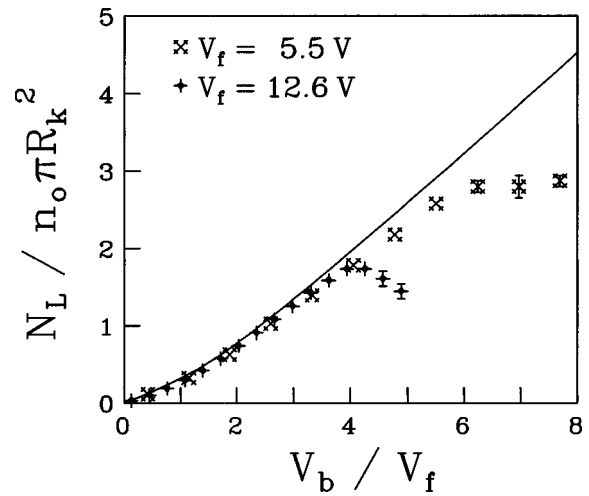


FIG. 6. Measured number of electrons per unit length N_L versus cathode bias V_b , for two different filament voltages V_f . Both N_L and V_b are effectively scaled by V_f , since $n_0 \propto V_f$ in Eq. (6). The theoretical curve is found by integrating the density profiles of Fig. 5 out to the cathode radius.

Fig. 2] would be visually indistinguishable from the curve in Fig. 6. That is, the total number of electrons in the plasma is basically independent of variations in cathode emission, despite the distribution of the electrons in the column, $n(r)/n(0)$, being strongly dependent on the emission profile. In essence, with sufficient cathode emission, electrons will fill the trap until the space-charge potential at $r=0$ becomes at least as negative as the bias potential.

In Fig. 7 a typical set of density profiles measured across the full diameter of the plasma column is shown. Each data point in Fig. 7 represents the average of eight shots, and the estimated error from shot-to-shot noise is typically smaller than the symbol size. For these data we have set $V_f = 12.6 \text{ V}$, and the different symbols correspond to different values of V_b . The radius of the column increases with in-

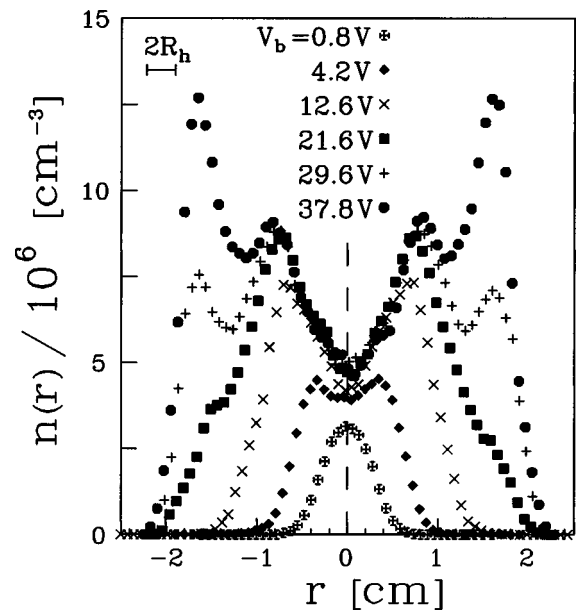


FIG. 7. Measured radial density profiles for $V_f = 12.6 \text{ V}$. The bar labeled $2R_h$ represents the diameter of the collimator hole.

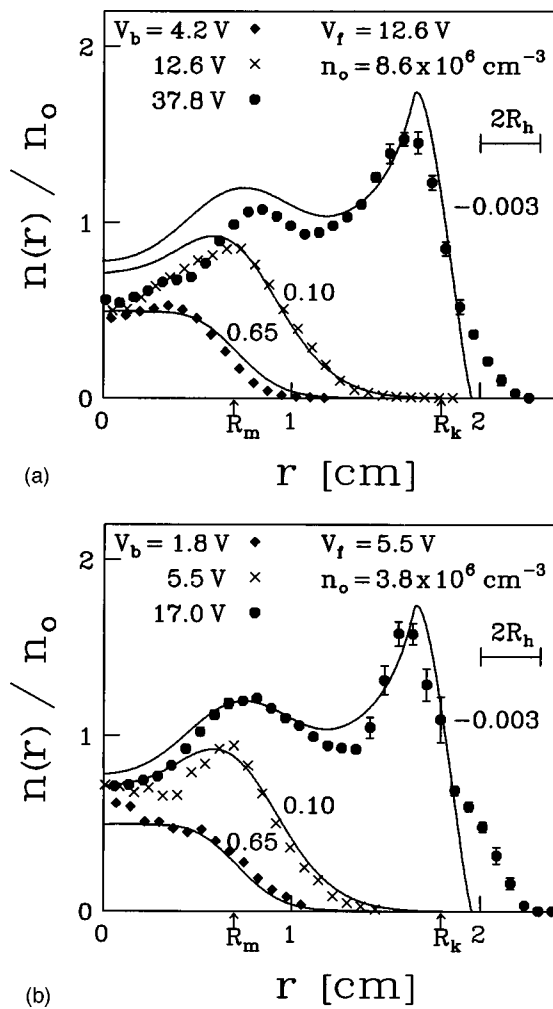


FIG. 8. Measured profiles with $V_b/V_f \approx 0.33, 1, \text{ and } 3$ for (a) $V_f = 12.6$ and (b) $V_f = 5.5$. The solid lines are theoretical predictions labeled by the value of the parameter γ^* .

creasing bias voltage until the column is approximately as wide as the cathode, at $V_b = 29.6$ V. A further increase in V_b causes electrons to ‘pile up’ at the edge of the column. For all but the smallest bias voltages, the profiles have multiple dips and peaks similar in shape to the curves shown in Fig. 5. The data also displays a high degree of side-to-side symmetry, indicating rotational smoothing of any azimuthal asymmetries in emission.

Figures 8(a) and 8(b) show measured profiles compared to predictions of the model with no adjustable parameters. Figure 8(a) shows part of three of the profiles from Fig. 7, with $V_f = 12.6$ V; Fig. 8(b) shows three partial profiles taken with $V_f = 5.5$ V. In each figure, the three measured profiles are at different values of V_b , and the ratio of V_b/V_f is used to determine the theoretical parameter γ (or γ^*). This value of γ^* then uniquely determines a predicted profile from the family shown in Fig. 5. The predicted profiles are identical for the two different values of V_f , because the ratios of V_b/V_f were chosen to be approximately the same in the experiments.

The theoretical curves given by the simple model reproduce the radial variations in the measured profiles, and ap-

proximately match the magnitude of the density. Thus, in an experiment with $R_k, R_w,$ and eV_f/T fixed we have three simple results: (1) V_f sets the density scale through the parameter n_o ; (2) $f_k(r)$ determines the radial profile shape of a family of curves (as in Fig. 5); and (3) V_b/V_f determines the scaled line density $N_L/n_o\pi R_k^2$ and central density $n(0)/n_o$, in effect picking one of the profile curves from the family.

For comparison to the measurements, the theoretical curves in Fig. 8 have been ‘convoluted’ so as to include the spatial averaging that occurs due to the finite radial size of the collimator hole. We also note that the ‘hollow’ columns shown in Figs. 7 and 8 will generally exhibit $\mathbf{E} \times \mathbf{B}$ shear-flow instabilities¹⁷ after being trapped, and the resulting turbulence would cause rapid relaxation to a stable, monotonically decreasing profile. The present theory only describes the initial density profile of the electron column immediately after it is isolated from the cathode.

As a final comparison between the model and the measurements we note that a theoretical limit for the scaled central density, $n(0)/n_o$, can be calculated using Eqs. (13) and (14) with $eV_f/T = 16$. For uniform cathode emission, this limit is $n(0)/n_o \leq 1.006$, and for the peaked cathode described by Eq. (18) the limit is $n(0)/n_o \leq 0.765$. Experimentally we find that $n(0)/n_o \leq 0.6-0.8$ for filament voltages in the range $V_f = 2.4-12.6$ V.

IV. DISCUSSION

In applying the theoretical model to the measured data, we used the relationship $T = eV_f/16$ for the thermal energy spread of the electrons. This relationship was found empirically by fitting the theoretical density profiles to the measured profiles near the column edge for a range in V_f between 2.4 and 12.6 V. The justification for this relationship was that the thermal energy spread is due to averaging over potential differences between points on the cathode, and is basically proportional to the turn-to-turn voltage difference. However, for a spiral filament the turn-to-turn voltage increases with radius, and throughout the paper we make the tacit assumption that T is uniform in radius. This last assumption is by no means a necessary assumption. The theoretical model assumes that the plasma is Maxwellian only along each axial field line, and electrons on separate field lines are not necessarily in thermal equilibrium with each other. In fact, the agreement between the theoretical and measured density profiles becomes even closer, primarily near $r = 0$, when the temperature is taken to be lower on center and increasing with radius. We take T to be uniform in an attempt to keep the model as simple as possible, while still capturing the basic features of the measured density profiles.

The assumptions of sufficient emission and a Maxwellian velocity distribution, however, are essential, and both assumptions break down when V_b is too large. The measured data shown in Fig. 6 begins to deviate from theory and the shot-to-shot noise increases when $V_b/V_f \gtrsim 4$. We believe that at these high bias voltages, the emission is no longer sufficient to maintain a steady-state column, and the electrons do not slow to a Maxwellian after the grid; that is,

$|\phi(r)| < |V_k(r)|$ in the containment region. When this occurs, the injection is beam-like; Eq. (1) is not valid; and the model ceases to be applicable.

It is not necessary to know the magnitude of the cathode emission $n_k(0)$ accurately in order to use this model. Uncertainty in $n_k(0)$ is inconsequential because this parameter enters only through the logarithmic term in Eq. (17). For instance, a uniform factor of 2 increase in $n_k(r)$ at all points along the cathode [i.e., $n_k(0) \rightarrow 2n_k(0)$, with $f_k(r)$ unchanged] would only cause a 1% increase in the theoretical density at any given radius, along with a 1% change in N_L .

In contrast to the weak dependence on $n_k(0)$, radial non-uniformities in emission strongly affect the shape of the density profile; that is, the model has a strong dependence on $f_k(r)$. For example, Figs. 2 and 5 show that the theoretical density profile from a cathode with an off-center factor of 2 peak in emission differs with that from a uniformly emitting cathode by as much as 30%, even though there is almost no difference in N_L for the two cases.

The importance of $f_k(r)$ and the unimportance of $n_k(0)$ is because the density of the electron column is local, whereas the potential is global. If the emission is relatively high at one radius, the plasma density is increased at that one particular radius, but the space-charge potential is made more negative at all radii. For example, a relative increase in density at $r=R_m$ leads to more electrons being reflected at $r=0$, with the final result being density profiles such as those in Figs. 5, 7, and 8.

The model we present considers only radial variations in emission; however, our experiment uses a spiral cathode with obvious theta variations. We find that our 1-D theory is most applicable to our 2-D emission when the $\mathbf{E} \times \mathbf{B}$ rotation time of the plasma, $\tau_{\mathbf{E} \times \mathbf{B}}$, is less than the time to close the injection gate, so that azimuthal asymmetries are smoothed out. In addition, the relative magnitudes of $\tau_{\mathbf{E} \times \mathbf{B}}$ and τ_b , where $\tau_b \equiv 2L/(T/m)^{1/2}$ is the axial bounce time, may also be an important consideration. For the measurements presented in this paper $\tau_{\mathbf{E} \times \mathbf{B}} \sim \tau_b$. However, in machines operating at higher magnetic fields ($B_z \gtrsim 4$ kG) the relationship $\tau_{\mathbf{E} \times \mathbf{B}} \gg \tau_b$ often holds. This inequality implies that electrons do not rotate in θ before bouncing back to the cathode. At

these higher fields the spiral shape of the filament can be observed in the trapped plasma,¹⁴ and the model fails to accurately predict the radial density profile. Theta smearing appears to be a necessary condition for our simple radial model to be applicable to spiral filaments.

Despite its simplicity, the 1-D model presented here accurately describes the injection process for our relatively low-field ($B_z = 380$ G) electron-plasma apparatus. We feel that the model can facilitate the design and operation of r^2 potential cathodes, in regimes where the injection is Maxwellian and azimuthally symmetric. The model could be particularly useful when applied to a cathode with a controllable emission profile, $f_k(r)$. In this case one could use the model to predict the parameters needed to produce a wide range of interesting initial density profiles, gaining the ability to easily tailor a plasma to fit the specific needs of a given experiment.

ACKNOWLEDGMENTS

This work was supported by Office of Naval Research Grant No. N00014-96-1-0239. We gratefully acknowledge the contributions of the late J. H. Malmberg in beginning this analytical model.

- ¹See, T. M. O'Neil, Phys. Scr. **T59**, 341 (1995), and references therein.
- ²*Non-Neutral Plasma Physics II*, edited by J. Fajans and D. Dubin AIP Conf. Proc. 331 (AIP, New York, 1995).
- ³J. H. Malmberg, Plasma Phys. Controlled Fusion **34**, 1767 (1992).
- ⁴I. Langmuir, Phys. Rev. **21**, 419 (1923); C. D. Child, *ibid.* **32**, 492 (1911).
- ⁵J. H. Malmberg and J. S. deGrassie, Phys. Rev. Lett. **35**, 577 (1975).
- ⁶C. F. Driscoll and J. H. Malmberg, Phys. Fluids **19**, 760 (1976).
- ⁷T. M. O'Neil and C. F. Driscoll, Phys. Fluids **22**, 266 (1979).
- ⁸R. C. Davidson, *Physics of Nonneutral Plasmas* (Addison-Wesley, New York, 1990), pp. 52–56.
- ⁹D. A. Moore, Ph.D. thesis, Princeton University, 1995.
- ¹⁰R. W. Gould and M. A. LaPointe, Phys. Fluids B **4**, 2038 (1992).
- ¹¹G. W. Hart, Phys. Fluids B **3**, 2987 (1991).
- ¹²D. L. Eggleston, Phys. Plasmas **1**, 3850 (1994).
- ¹³For a review of antimatter sources, see R. G. Greaves and C. M. Surko, Phys. Plasmas **4**, 1528 (1997).
- ¹⁴K. S. Fine, A. C. Cass, W. G. Flynn, and C. F. Driscoll, Phys. Rev. Lett. **75**, 3277 (1995).
- ¹⁵D. R. Durkin and J. Fajans, Bull. Am. Phys. Soc. **41**, 1521 (1996).
- ¹⁶S. Dushman, Phys. Rev. **21**, 623 (1923).
- ¹⁷C. F. Driscoll and K. S. Fine, Phys. Fluids B **2**, 1359 (1990).